

Article

Development of a Fusion Framework for Lithium-Ion Battery Capacity Estimation in Electric Vehicles

Bo Jiang¹, Xuezhe Wei² and Haifeng Dai^{2,*}

¹ Postdoctoral Station of Mechanical Engineering, School of Automotive Studies, Tongji University, Shanghai 201804, China

² Clean Energy Automotive Engineering Center, School of Automotive Studies, Tongji University, Shanghai 201804, China

* Correspondence: tongjidai@tongji.edu.cn

Abstract: The performance of a battery system is critical to the development of electric vehicles (EVs). Battery capacity decays with the use of EVs and an advanced onboard battery management system is required to estimate battery capacity accurately. However, the acquired capacity suffers from poor accuracy caused by the inadequate utilization of battery information and the limitation of a single estimation method. This paper investigates an innovative fusion method based on the information fusion technique for battery capacity estimation, considering the actual working conditions of EVs. Firstly, a general framework for battery capacity estimation and fusion is proposed and two conventional capacity estimation methods running in different EV operating conditions are revisited. The error covariance of different estimations is deduced to evaluate the estimation uncertainties. Then, a fusion state-space function is constructed and realized through the Kalman filter to achieve the adaptive fusion of multi-dimensional capacity estimation. Several experiments simulating the actual battery operations in EVs are designed and performed to validate the proposed method. Experimental results show that the proposed method performs better than conventional methods, obtaining more accurate and stable capacity estimation under different aging statuses. Finally, a practical judgment criterion for the current deviation fault is proposed based on fusion capacity.



Citation: Jiang, B.; Wei, X.; Dai, H. Development of a Fusion Framework for Lithium-Ion Battery Capacity Estimation in Electric Vehicles. *Batteries* **2022**, *8*, 112. <https://doi.org/10.3390/batteries8090112>

Academic Editor: King Jet Tseng

Received: 22 July 2022

Accepted: 30 August 2022

Published: 5 September 2022

Publisher's Note: MDPI stays neutral with regard to jurisdictional claims in published maps and institutional affiliations.



Copyright: © 2022 by the authors. Licensee MDPI, Basel, Switzerland. This article is an open access article distributed under the terms and conditions of the Creative Commons Attribution (CC BY) license (<https://creativecommons.org/licenses/by/4.0/>).

1. Introduction

The rapid development of new energy vehicles benefits from the desire to reduce emissions and pollution [1]. Among different new energy vehicles, electric vehicles (EVs) are the most promising for mass commercialization, which gives credit to the excellent performance of lithium-ion batteries (LIBs) [2]. LIBs have the superiority of high power/energy density, light weight, and long life cycle [3]. However, their adaptability to the harsh working environment, poor thermal safety, and inevitable degradation need scientific improvements. The solution to the above challenges can be achieved through the battery design, for example, improvements in battery electrodes [4,5] and efficient battery management technologies for battery systems [6,7]. High-performance battery management technologies are an essential impetus for the development of EVs.

Among battery management technologies, LIB capacity is a vital parameter for characterizing battery performance and is deemed a direct indicator of battery health level [8]. Battery capacity affects the uninterrupted driving range of EVs and is a prerequisite for estimating some essential battery internal states. However, battery capacity is time varying and decays as the battery ages [9], which will challenge the capability of state estimation; hence, exact capacity information is essential for better management and utilization of LIBs. The direct measurement method is the most accurate to obtain battery capacity; however,

this method is time consuming and usually limited by the operating conditions, which is unsuitable for real EV applications [10]. Therefore, accurate onboard estimation of battery capacity is a research hotspot in battery management technologies in EVs.

1.1. Review of Existing Battery Capacity Estimation Approaches

Many studies have investigated indirect estimation methods of battery capacity for EVs [11–13]. Generally, commonly used battery capacity estimation approaches categorize into three classes: the method based on the state of charge (SOC), the method based on incremental capacity analysis (ICA), and the data-driven method.

It can be found that SOC has a close relationship with battery capacity and the SOC-based methods utilize the change in SOC and charge accumulation over a while to estimate battery capacity [14]. Some researchers employed the measured or estimated open-circuit voltage to obtain SOC and achieve battery capacity [15,16]. Considering that battery capacity can be regarded as an unknown parameter, some joint estimation techniques for battery SOC and capacity are springing up. A single state vector containing battery SOC, capacity, and other parameters and corresponding state-space function was established to estimate battery capacity [17,18]. Using two or more estimators is more flexible and has been investigated by many researchers. Dual extended Kalman filter [19], dual sliding-mode observer [20], dual nonlinear predictive filter [21], and Kalman filter together with least squares [22] are common attempts to achieve the co-estimation. Battery SOC is fundamental in battery management technology, so the SOC-based capacity estimation method is accessible to implement. Some factors, including the SOC estimation error and the different time-varying characteristics between states, shall be considered when using this method [23].

The ICA method is another practical capacity estimation method, using the differential technology to transfer the battery charging capacity voltage (Q-V) curve into the incremental capacity (IC) curve. The features of the IC curve indicate the battery's internal electrode behavior; therefore, this method can analyze the battery aging mechanism [24]. A close relationship between IC curve features and battery health status can be established and further used for online capacity estimation. A necessary procedure in ICA technology is curve fitting/smoothing because the differential operation in ICA technology is sensitive to measurement noise. He et al. [25] compared six commonly used voltage curve fitting models in IC curve determination and the model in [26] was validated to be optimal for different types of batteries. After numerical differentiation, Gaussian filtering has an advantage over conventional moving average filtering in terms of IC curve smoothing [24,27], where low-frequency signals can be separated from high-frequency noise. An operating condition with a monotonic voltage change is necessary for ICA technology, limiting the application of this method.

The data-driven method has been widely employed in battery state estimation with the development of artificial intelligence technology, allowing knowledge related to battery aging to be learned from battery training datasets and further used for online capacity estimation [28,29]. Feature engineering is the first step in a data-driven estimation method. Compared with the discharging condition, the battery charging condition is more stable and regular and is usually used to extract battery-capacity-related features. Five charging-related features, including the initial and final charge voltage, the final charge current, the constant current charge capacity, and the constant voltage charge capacity, were extracted from charge curves [30]. After determining battery features, machine learning algorithms, including kernel techniques [31,32] and neural-network techniques [28,33], are employed to estimate capacity. The main concern during the online application of this method is the high computational effort.

Except for the above typical capacity estimation methods, fusion technologies have also been widely employed in battery state estimation. Zheng et al. [34] studied a novel capacity estimation method with the help of fusion estimation of battery charging curves and the Arrhenius aging model, which shows high estimation accuracy over the whole

battery lifecycle. A multi-stage fusion method containing three battery models at different aging levels was proposed by Xiong et al. [35] and then the residual error of each model was employed to calculate the fusion weight. Moreover, Balasingam et al. [36] investigated a robust capacity estimation fusion method, which can optimally utilize the estimates from different approaches; however, only simulation data were used for validation in this work. Owing to the effective utilization of more information from different sources, the information fusion techniques can not only eliminate noise and outliers in the input information but also achieve a complete description of the observed object through information complementarity [37]. The multi-source information represents the data from different models [35], different approaches [34,36], and different operating scenes. Using the multi-source information, the fusion techniques promise to improve the estimation accuracy and enhance the estimation stability.

1.2. Existing Challenges and Original Contributions

The above overviews several typical capacity estimation methods and each approach shows better performance under specific conditions. However, the following issues remain to be addressed among current capacity estimation methods.

(1) *The inadequate utilization of battery information.* The attenuation of battery capacity affects the dynamic trajectories of other battery states, including SOC, terminal voltage, and open-circuit voltage. This inspires researchers to perform capacity estimation using the variation in the above states combined with the battery current. However, one primary shortage in the above approaches is that only a single battery information source (except battery current) is utilized in capacity estimation. For example, the SOC-based method only utilizes the battery SOC and current, while the ICA-based method only uses the battery voltage and current. The inadequate utilization of battery information could lead to difficulties in improving the estimation accuracy.

(2) *The limitation of EVs' operating conditions on estimation methods.* As introduced above, each method may only adapt to a specific operating condition. For the ICA-based and data-driven methods, the EV charging condition is stable and suitable for feature construction. In contrast, the EV discharging condition is random, not monotonous, and not convenient for the online application of these two methods. The adaptive filters offer advantages in SOC acquisition to the SOC-based method and battery model parameter determination is an important step. In this situation, dynamic discharging will be helpful because of adequate current excitation for parameter identification. Therefore, the battery operating conditions may limit the above capacity estimation methods.

(3) *The weak anti-interference ability to the system error.* Another deficiency in traditional capacity estimation is the weak anti-interference ability to system error because only one estimation approach is employed. Battery current is the critical information in capacity estimation and inaccurate current information affects the estimation accuracy. For example, a micro-internal short circuit (ISC) is a severe battery failure and may cause a thermal runaway of LIBs [38,39]. Supposing a battery has a micro-ISC fault (inaccurate current information), the SOC-based method may obtain a smaller capacity estimate, while the ICA-based method may get a larger capacity estimate. Hence, the weak anti-interference ability to system error may lead to capacity estimation deviations.

Considering the above problems, this study proposes an adaptive fusion method for battery capacity estimation under actual EV operation conditions, which takes advantage of information fusion technologies. Concretely, the SOC-based and ICA-based capacity estimation constitutes the fusion method, which can fully utilize battery information, including the battery current, SOC, and voltage. Moreover, the two base estimators operate in different working conditions, achieving the fusion framework during complete operating conditions. Here, the complete operating condition means the combination of discharging and charging conditions, which simulates the actual working conditions of EVs. The fusion of different capacity estimations enhances the anti-interference ability against system error because these two base estimators have different estimation characteristics under inaccur-

rate battery current information. In our previous work, presented in VPPC 2020, Gijon, Spain [40], this framework was initially introduced and verified with a fresh battery cell. Significant extensions are provided in this study. Specifically, an improved estimation and fusion framework is investigated, in which the noise-compensating method is employed for capacity estimation during discharging. Moreover, the constructed fusion framework is validated by experimental data of aged battery cells and with inaccurate current information. The main work in this paper can be generalized as follows. Firstly, a general framework for battery capacity estimation and fusion is proposed, then the SOC-based and ICA-based capacity estimation approaches are revisited in different operating conditions and the corresponding error covariance of the two estimates is obtained separately. The acquisition of the fusion capacity is realized through the Kalman filter. Laboratory experiments simulating the EV operating conditions are designed and performed to validate the effectiveness of the proposed fusion method under different dynamic conditions and aging statuses. Furthermore, a practical judgment criterion for the current deviation fault is proposed based on fusion capacity.

1.3. Outline of the Paper

The remainder of this paper is organized as follows. Section 2 proposes the general estimation and fusion framework and derives the uncertainties of capacity estimation from two estimation approaches; further, the adaptive fusion of two estimations is constructed. The test bench and designed battery experiments are shown in Section 3. Section 4 shows the experimental results and discusses the accuracy and robustness of the fusion method. Finally, Section 5 concludes this paper.

2. Multi-Dimensional Capacity Estimation and Fusion

2.1. Development of the Adaptive Fusion Framework

Aiming to realize the adaptive fusion for capacity estimation, a general framework for battery capacity estimation and fusion is shown in Figure 1a. Three main procedures are included in the general framework: multi-dimensional capacity estimation, determination of estimation uncertainty, and fusion center.

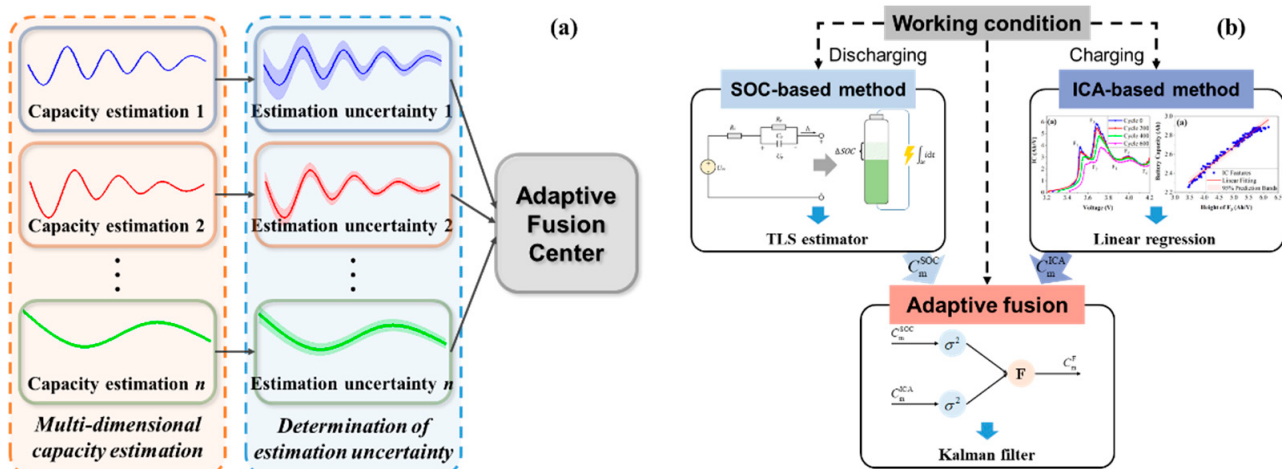


Figure 1. Battery capacity estimation and fusion. (a) A general framework of multi-dimensional capacity fusion. (b) The specific implementation in this study.

The multi-dimensional capacity estimation originates from the traditional methods listed in the literature review. With the increment of onboard chips' computing ability and improvement in estimation algorithms, multiple estimation methods can run simultaneously and export estimated capacity from different dimensions. Multi-dimensional capacity estimation brings opportunities for improving estimation accuracy because of the increase in useful information. The second step is the determination of estimation uncertainty.

Except for the estimated values, the estimated uncertainties are also essential knowledge in capacity fusion. The estimated uncertainties reflect the estimation error characteristics for estimated values and contribute to the adaptive filter-based fusion. The final is the adaptive fusion center, which receives information from all the capacity estimators and some adaptive fusion algorithms can be utilized for capacity fusion in the fusion center. The framework shown in Figure 1a is a centralized fusion system and the weighted average filter, least squares, and Kalman filter are common technologies in information fusion.

During the fusion process, a state-space function is established to describe the battery capacity characteristics. Battery capacity is a slowly varying state and can be further assumed to be disturbed by Gaussian white noise. The following equation is satisfied:

$$\mathbf{x}_{l+1} = \boldsymbol{\phi}\mathbf{x}_l + \mathbf{w}_l \quad (1)$$

where \mathbf{x}_l represents the l th fusion state, $\boldsymbol{\phi}$ is the system matrix, and \mathbf{w}_l is the system noise during the fusion process and is considered a Gaussian white noise with covariance Q_l .

Two structures are usually employed in the fusion center: parallel structure and sequential structure. The parallel structure handles the independent estimated values from the transmitting sub-system simultaneously, while the sequential structure successively deals with the corresponding estimated values. The fusion measurement function can be expressed as:

$$\mathbf{z}_l = \mathbf{H}\mathbf{x}_l + \mathbf{v}_l \quad (2)$$

where \mathbf{z}_l estimated capacities and \mathbf{z}_l^i comes from the i th sub-system, \mathbf{H} is the output matrix, and \mathbf{v}_l is corresponding measurement noise with covariance R_l^i .

It has been approved that parallel structure-based and sequential structure-based fusion have the same estimation accuracy [41]. Based on the constructed state-space function, some adaptive filters can obtain the optimal fusion state. Finally, the capacity fusion based on multi-dimensional estimation will be achieved.

According to the above general battery fusion methodology, together with the vision of utilizing more battery information effectively and taking advantage of battery operating conditions, a specific implementation is shown in Figure 1b. Inspired by Ref. [36], the proposed method will utilize more battery information effectively by combining the characteristics of battery operations. Generally, the implementation of capacity fusion is based on the sequential structure. It contains three main parts: (1) the SOC-based estimation during the dynamic discharging, (2) the ICA-based estimation under the stable charging condition, and (3) the final adaptive fusion under complete operating conditions. The first two parts have been preliminarily studied in our previous works [42,43]. This study will further revisit these two methods and obtain the estimation uncertainties, which will be used for adaptive fusion.

2.2. Revisiting Capacity Estimation at Different Working Conditions

2.2.1. SOC-Based Estimation during the Discharging Condition

The definition of battery SOC can be rewritten as

$$\sum_{k=k_1}^{k=k_2} i_k \Delta t = C_m \times (\text{SOC}_{k_1} - \text{SOC}_{k_2}) \quad (3)$$

where k_1 and k_2 are different sampling points, Δt is the sampling time, i_k is the battery current, and C_m is the battery capacity. Defining SOC change as $X = \text{SOC}_{k_1} - \text{SOC}_{k_2}$ and charge accumulation as $Y = \sum_{k=k_1}^{k=k_2} i_k \Delta t$, Equation (3) can be transformed to $Y = C_m X$. If N observations are performed for X and Y , the following equation in vector form can be obtained:

$$\mathbf{Y} = C_m \mathbf{X} \quad (4)$$

where $\mathbf{X} = [X_1, X_2, \dots, X_N]^T$ and $\mathbf{Y} = [Y_1, Y_2, \dots, Y_N]^T$.

The traditional least-squares method can be used for the solution of Equation (4), if the system data are accurate enough. However, the system input X and output Y may be noisy, for example, disturbed by the measurement and estimation noise. The noisy data can be expressed as

$$\begin{cases} X = \tilde{X} + \varepsilon_X \\ Y = \tilde{Y} + \varepsilon_Y \end{cases} \quad (5)$$

where \tilde{X} and \tilde{Y} are real values and ε_X and ε_Y are supposed to be zero-mean Gaussian white noises, respectively. The former noise mainly comes from the SOC estimation uncertainty, while the current measurement noise and numerical computation error will lead to the noise on Y . Under these circumstances, the conventional least-squares method is biased and unsuitable for online capacity estimation.

The total least squares (TLS) is a useful technique for such a system with noisy data [43–45]. In our previous study [43], co-estimation of battery SOC and capacity is realized. The joint estimation consists of an adaptive extended Kalman filter (AEKF) and a TLS estimator and uses a Thevenin model to describe the battery dynamic characteristic. When the AEKF estimator outputs the battery SOC, the TLS algorithm can perform the capacity estimation according to Equation (4). A Rayleigh-Quotient based TLS is employed to realize the recursive running of capacity estimation. The minimum of the following Rayleigh-Quotient function is the solution of the TLS estimator.

$$J(\theta_n, \bar{R}_n) = \frac{\theta_n^T \bar{R}_n \theta_n}{\theta_n^T \theta_n} \quad (6)$$

where $\theta_n = [C_m - 1]^T$, \bar{R}_n is the autocorrelation matrix of the augmented data matrix $H = [X \ Y]^T$. A gradient-based method is employed for recursively updating the C_m [45], where $C_{m,n} = C_{m,n-1} + \alpha_n X_n$ and α_n is to minimize the gradient of Equation (6).

The above procedures realize the capacity estimation during EV discharging and will be considered one of the essential inputs for capacity fusion.

2.2.2. ICA-Based Estimation during the Charging Condition

Employing differential technology, the ICA method can distinguish the voltage characteristics influenced by battery degradation. The ICA technique is usually adopted to investigate the battery aging mechanism [46]. For online capacity estimation, the ICA equation can be rewritten in a discrete form as

$$IC = \frac{dQ}{dV} \approx \frac{\Delta Q}{\Delta V} = \frac{Q_2 - Q_1}{\Delta V} = \frac{i\Delta T}{V_2 - V_1} \quad (7)$$

where ΔV and ΔT are the voltage interval and time interval to calculate the IC value, separately. The problem is that the selection of ΔV and ΔT is not adaptive and the IC curve will be susceptible to measurement noise. In our previous work [42], a filter-based method was proposed to generate the IC curves and this method showed good effectiveness and less computational cost.

Figure 2 shows the collected IC curves at different cycles under different aging conditions. Therefore, “0.5C–0.5C aging condition” means the accelerated cyclic aging test uses a 0.5C current for charging, followed by a 0.5C current for discharging. The IC curves show similar shapes, even at different aging cycles with different aging conditions. During battery charging, six noticeable features (noted as F_1 ~ F_6 , including peaks and valleys) on the IC curves can be found. It should be noted that this is only one typical method for extracting features from IC curves. Dubarry et al. [47,48] presented a comprehensive summary of features of interest with battery SOH for different kinds of batteries, including the area, position, and intensity of the IC curves. In this study, with the increase in aging cycles, the battery IC curves shift significantly downwards and slightly towards higher

voltage, which means that the IC curve features have a close relationship with battery aging and can estimate battery capacity.

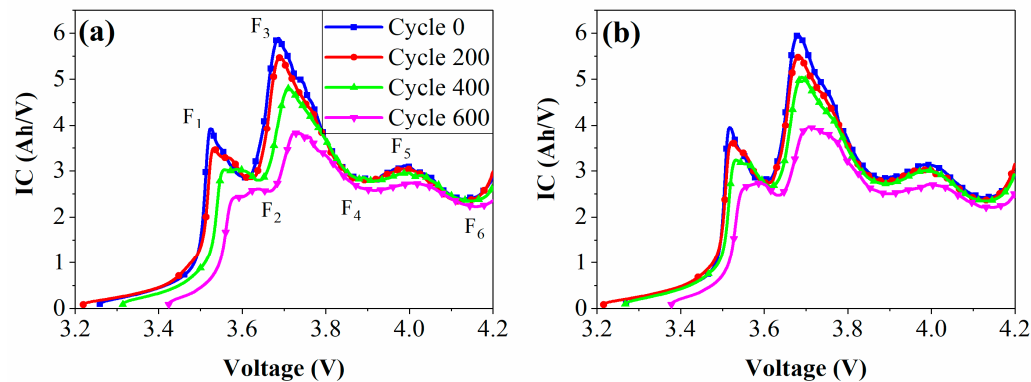


Figure 2. Battery IC curves at different aging cycles. (a) 0.5C-0.5C aging condition. (b) 0.5C-1C aging condition.

In this study, the height of these features is used for relationship construction because battery aging has less impact on the position of these features. Considering that when the battery is seriously aged (aging cycle ≥ 600), F₁ and F₂ blend together, which is difficult to identify and unsuitable for capacity, only F₃ to F₆ are taken into account in the following discussion.

It has been confirmed that the height of the IC features is linearly correlated to battery aging (Figure 3). The relationship between these features and battery capacity is constructed based on linear regression (LR), as shown in the following equation

$$C_m^{\text{ICA}} = \alpha_i \times H_{F_i} + \beta_i + \varepsilon_i \quad (8)$$

where H_{F_i} is the height of i th IC features; α_i and β_i are the regression coefficients; ε_i is the error term with zero-mean and variance σ_i^2 .

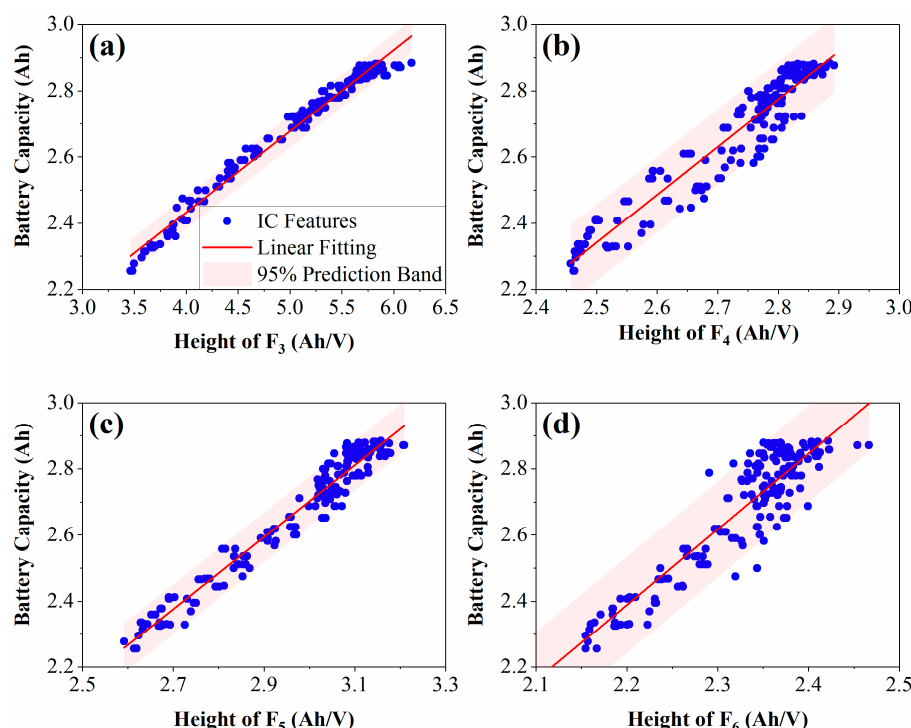


Figure 3. The linear relationship and prediction bands of the ICA method. (a–d) are the diagrams of F₃–F₆, separately.

2.3. Adaptive Capacity Fusion during Complete Operating Conditions

The above content discusses two capacity estimation methods, which mainly use different information and operate under different EV operating conditions. Inspired by the multi-source information fusion theory, this study investigates capacity fusion under complete operating conditions to acquire a more accurate and reliable capacity estimate.

Equations (1) and (2) show the state-space function of the sequential structure-based fusion. Either the estimated value from the SOC-based method or the ICA-based method can be regarded as an “observation” of the battery’s actual capacity. Hence, two estimates (C_m^{SOC} and C_m^{ICA}) can be considered as the actual capacity disturbed by noise. As shown in Figure 1b, during the discharging process, $z_l = C_m^{\text{SOC}}$ and, during the charging process, $z_l = C_m^{\text{ICA}}$. Correspondingly, R_l is selected from the uncertainties according to the operating conditions.

For SOC-based estimation, C_m^{SOC} is realized through the TLS method. Crassidis et al. [49] derived that the error covariance matrix P of estimated parameters in the TLS problem is the inverse of the Fisher information matrix F ($P = F^{-1}$) and gave the approximate error covariance. Hence, in this study, the uncertainty of the SOC-based estimation is shown as follows

$$R^{\text{SOC}} = \left(\frac{1}{\theta_n^T R_n \theta_n} \sum_{i=1}^n X_i X_i^T \right)^{-1} \quad (9)$$

where R^{SOC} is the error covariance of estimated C_m^{SOC} ; other variables have the same meanings as in Equation (6).

For the ICA-based method, C_m^{ICA} is realized through the LR method. Equation (8) can be rewritten in a general form as $y = \alpha x + \beta + \varepsilon$, where x and y are the regression input and output. As shown in [50], the estimation of error variance σ^2 can be calculated as

$$\hat{\sigma}^2 = \frac{1}{N_{\text{LR}} - 2} (S_{yy} - \hat{\alpha} S_{xy}) \quad (10)$$

where N_{LR} represents the number of points used for regression, $\hat{\alpha}$ is the estimation of α ; $S_{xy} = \sum (x_i - \bar{x})(y_i - \bar{y})$ and $S_{yy} = \sum (y_i - \bar{y})^2$, where S_{xy} is the sum of the deviation product of x and y and S_{yy} is the sum of the deviation square of y .

The estimation error covariance of the LR method can be expressed as

$$R^{\text{ICA}} = [1 + \frac{1}{N_{\text{LR}}} + \frac{(x' - \bar{x})^2}{S_{xx}}] \hat{\sigma}^2 \quad (11)$$

where $S_{xx} = \sum (x_i - \bar{x})^2$ is the sum of the deviation square of x . In the ICA-based method, $x = H_F$ and x' means the features obtained online.

Figure 3 shows the linear correlation between actual capacity and heights of IC features and the 95% prediction band of the LR method is also shown. Here, the prediction band is calculated based on Equation (11). It can be seen that the prediction band of F_4 and F_6 is broader than that of F_3 and F_5 , which means that the error covariance of F_4 and F_6 will be larger than others.

The above obtains the estimation uncertainties of two methods and the complete state-space function is constructed. Due to the simplicity of the state-space function, the Kalman filter is utilized for state fusion, which has superior performance and is easy to implement. For detailed procedures of the Kalman filter, refer to [8,22].

3. Experimental Setups and Design

The battery test bench includes a battery test system to implement charging and discharging procedures, a thermal chamber to provide uniform environmental temperature and humidity, and a host computer for data logging. A kind of commercial 18650-type battery (the cathode is $\text{LiNi}_{0.8}\text{Mn}_{0.1}\text{Co}_{0.1}\text{O}_2$ and the anode is graphite) is used in this study. The nominal capacity is 2.9 Ah and the charge/discharge cut-off voltages are 4.2 V and

2.5 V, respectively. During the experiments, the battery temperature is maintained at 25 °C. The battery experiment is designed to simulate the actual operation of the onboard battery as much as possible and validate the fusion method, as shown in Figure 4.

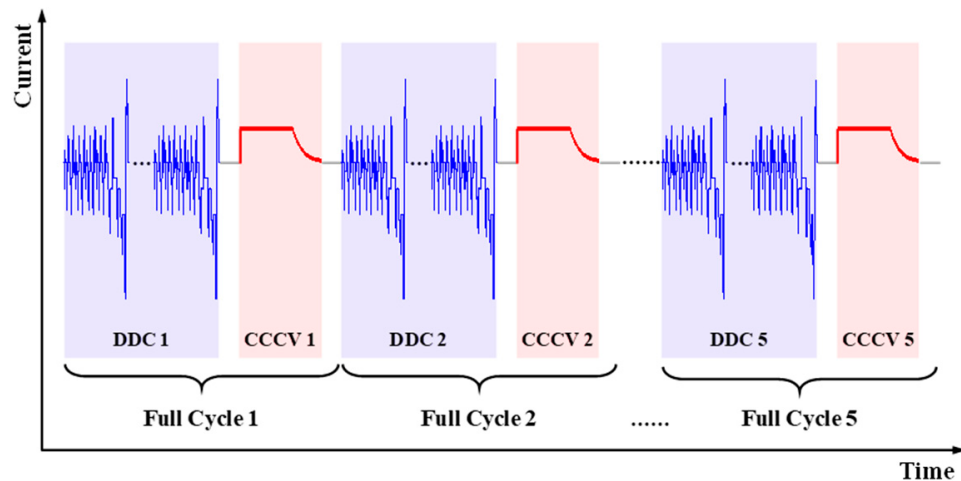


Figure 4. The current profiles of the designed experiment.

The battery will discharge to cut-off voltage with a dynamic discharging condition (DDC), followed by a constant current-constant voltage (CCCV) charging to 100% SOC, where the constant charging current is 1.375 A and the cut-off current for the CCCV protocol is about 60 mA. A DDC and a CCCV form a complete operating cycle and the whole experiment contains five complete cycles (notes as complete cycle 1–5). To verify the adaptability of the proposed method, three cells with different aging statuses are employed in this study, as shown in Table 1. During the experiments, Cell 1 and 2 will discharge with the new European driving cycle (NEDC) and Cell 3 will discharge with the Urban Dynamometer Driving Schedule (UDDS). The detailed current profiles of NEDC and UDDS can be found in Ref. [51]. Table 1 also shows the battery's actual capacity. The battery SOH is determined as the ratio of residual capacity to the nominal capacity [32,52].

Table 1. Cells used in the experiments.

Cell No.	Capacity	SOH	DDC
Cell 1	2.881 Ah	99.34%	NEDC
Cell 2	2.729 Ah	94.11%	NEDC
Cell 3	2.537 Ah	87.48%	UDDS

4. Results and Discussion

To evaluate the performance of the capacity fusion technique effectively, two general error criteria, including the maximum absolute percentage error (MaxAPE) and the root mean square error (RMSE), are adopted. The definition of these two criteria is shown as follows. The percentage error is used when calculating the RMSE.

$$\begin{cases} \text{MaxAPE} = \max\left(\left|\frac{\hat{y}_i - y_i}{y_i}\right|\right) \times 100\% \\ \text{RMSE} = \sqrt{\frac{1}{m} \sum_{i=1}^m \left(\frac{\hat{y}_i - y_i}{y_i}\right)^2} \times 100\% \end{cases} \quad (12)$$

where \hat{y} and y are the estimated and actual battery capacity and m represents the number of capacity estimates used for assessment.

4.1. Effectiveness of the Proposed Capacity Fusion

The effectiveness of the capacity fusion technique will be first verified based on the experimental data for Cell 1. Figure 5 shows the estimation and fusion results.

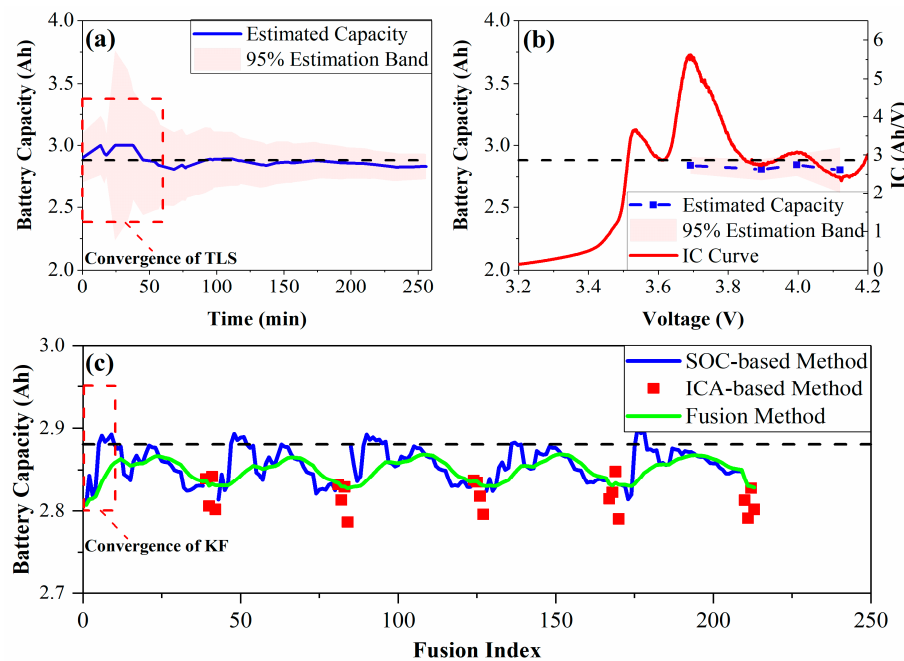


Figure 5. The capacity estimation and fusion results of Cell 1. (a) The estimated capacity and uncertainty from SOC-based method during DDC 1. (b) The estimated capacity and uncertainty from ICA-based method during CCCV 1. (c) The fusion results during 5 complete cycles.

When using the TLS estimator during DDC, the initial capacity is set to 2.9 Ah. Actually, this initial value has little influence on capacity estimation. Moreover, to prevent the influence of outliers on capacity estimation, the maximum value during recursion is set to 3.0 Ah. The estimation result during DDC 1 is shown in Figure 5a. The first several values have large deviations from the actual capacity (the dashed line represents the actual battery capacity). After convergence (about 2500 s for this condition), the estimated capacity becomes stable and close to the actual capacity. In addition, the 95% estimation band becomes narrower after convergence, which means the estimation uncertainties gradually decrease. Specifically, the convergence time of TLS is set to 1h and the estimated values before convergence will not be considered during fusion. After convergence, the MaxAPE and RMSE during DDC 1 are 2.558% and 1.195%, separately, indicating the effectiveness of the SOC-based method.

The estimation result of the ICA method during CCCV 1 is shown in Figure 5b. The capacity estimated through the last feature (F_6) has the biggest uncertainty. The MaxAPE and RMSE are 2.747% and 2.135%, which shows insufficient accuracy compared to the SOC-based method. Another shortcoming is that too few capacity values are updated based on IC curve features.

For the capacity fusion, the initial parameters of the Kalman filter during fusion are set to: $P_0 = 5 \times 10^{-3}$, $Q_l = 10^{-4}$, and R_l is calculated according to Equations (9) and (11). The capacity fusion result during the five complete cycles is shown in Figure 5c. It can be found that most of the estimated values of the SOC-based and ICA-based methods are smaller than the actual capacity. Through the Kalman filter, the trajectory of fusion capacity has fewer fluctuations. In most cases, the fusion value follows the estimates from the SOC-based method. However, when the uncertainty of the SOC-based method is considerable or the observations come from the ICA-based method, the trajectory of fusion capacity will change. Moreover, the ICA-based method has a larger estimation deviation and the fusion method can endure these errors. The first ten values during fusion are considered the Kalman filter's convergence process and will be ignored when assessing the performance. During five complete cycles, the MaxAPEs of SOC-based and ICA-based methods are 2.328% and 3.278%, while the MaxAPE of the fusion method is 1.862%, which is reduced by 0.466% and 1.416%, separately, compared with the above single method. It is

noted that the ICA-based method has few estimates, which influences the performance of the fusion method.

4.2. Adaptability to Different Aging Statuses

To validate the adaptability of the fusion method, another two cells with larger capacity attenuation are employed to perform the capacity fusion, as shown in Figure 6. Figure 6a shows the experimental results of Cell 2. The fusion capacity is closest to the battery's actual capacity. At the beginning of each DDC, the TLS estimator exports some outliers, which results in a significant estimation error. On the contrary, the fusion method utilizes the information from the ICA-based method and the uncertainty from the SOC-based method and obtains a more accurate and stable estimation result. In addition, some inaccurate estimates from the ICA-based method were also corrected. The MaxAPE is reduced by 1.478% and 0.985%, separately, compared with the SOC-based and ICA-based methods, while the RMSE is reduced by 0.307% and 1.100%.

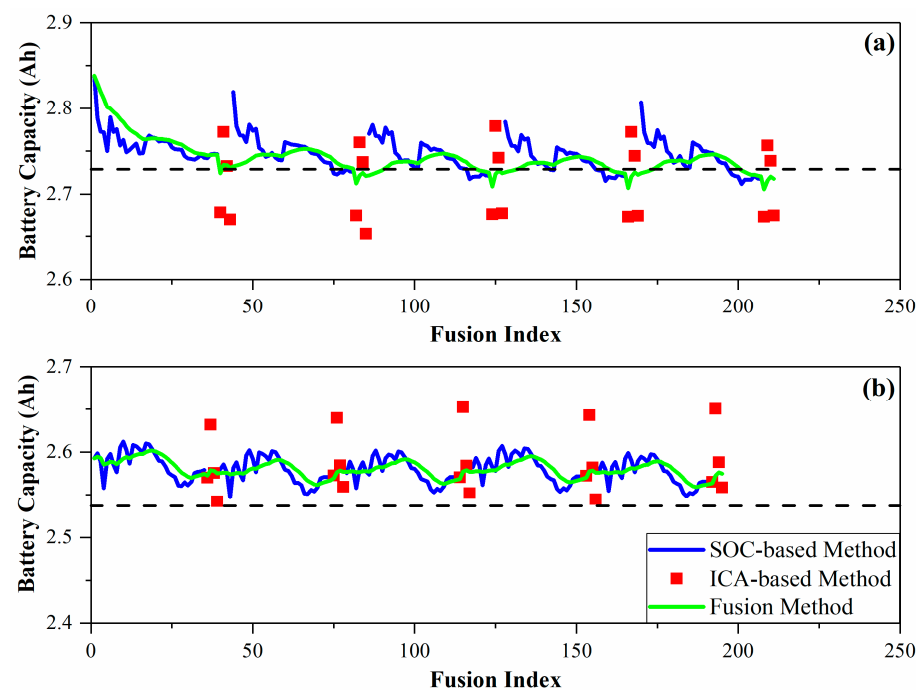


Figure 6. The estimation and fusion results of different cells. (a,b) are the results of Cell 2 and Cell 3.

The estimation results of Cell 3 are shown in Figure 6b. Unlike previous results for the other two cells, most of the estimated values for the SOC-based and ICA-based methods are larger than the actual capacity. Under such circumstances, the fusion method filters some outliers generated from the ICA-based method and obtains a smoother capacity estimation curve. During the five complete operating cycles, the MaxAPEs of the SOC-based, ICA-based, and fusion methods are 2.876%, 4.542%, and 2.547%. Compared with the single ICA-based method, the accuracy improvement in the fusion method is considerable.

Table 2 shows the estimation performance of different methods for cells with different aging statuses. For these three cells, the maximum MaxAPE and RMSE of the SOC-based method are 3.298% and 1.780% and those of the ICA-based method are 4.542% and 2.401%, while for the proposed fusion method, the maximum MaxAPE and RMSE are 2.547% and 1.703%, separately. The proposed fusion methods show the highest estimation accuracy from the capacity estimation results, indicating the adaptability to different aging statuses. It has been mentioned in Section 2.1 that the average filter is also a common technology in information fusion. Therefore, we compare the proposed fusion using the Kalman filter and traditional fusion using the moving average filter, as shown in Table 2. The window size for the moving average filter is 5. From Table 2, it can be found that moving

average fusion also improves the estimation performance compared with SOC-based and ICA-based methods. Nevertheless, it only uses the estimation value while ignoring the estimation uncertainty. Comparatively, the proposed fusion method using the Kalman filter still has a minor estimation error, indicating the effectiveness of the proposed method.

Table 2. The performance of different methods for different cells.

Method	Criterion	Cell 1	Cell 2	Cell 3
SOC-based method	MaxAPE (%)	2.328	3.298	2.876
	RMSE (%)	1.061	0.882	1.780
ICA-based method	MaxAPE (%)	3.278	2.805	4.542
	RMSE (%)	2.300	1.675	2.401
Fusion method: Kalman filter	MaxAPE (%)	1.862	1.820	2.547
	RMSE (%)	1.144	0.575	1.703
Fusion method: Moving average	MaxAPE (%)	2.239	1.823	2.698
	RMSE (%)	1.141	0.751	1.788

4.3. Application with Inaccurate Battery Current Information

As discussed above, inaccurate current information will result in errors in capacity estimation and different estimation methods may have different error scenarios. For a battery with an early ISC fault, the measured current is larger than the battery's effective current during charging. In contrast, during discharging, the measured current is less than the battery's effective current. In this situation, for the SOC-based method, although the SOC estimator may obtain relatively accurate SOC based on the feedback of measurement voltage, the calculated charge accumulation is less than the actual value, which will further result in a smaller capacity estimate. For the ICA-based method during charging, the calculated IC value according to the measured current will be larger than its actual value; thus, the capacity estimation based on IC features will be larger.

This section simulates two fault scenarios; one is with a 10 mA current deviation (noted as Fault 1) and the other is with a 20 mA current deviation (noted as Fault 2). The experimental data for Cell 1 are used for fault simulation. Figure 7 shows the capacity estimation and fusion results.

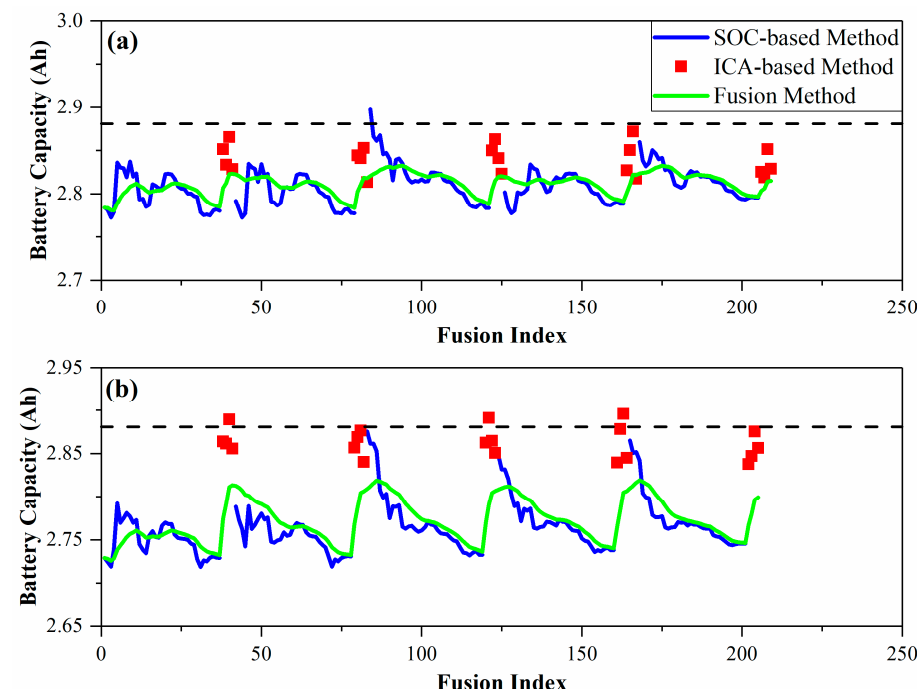


Figure 7. The estimation and fusion results of different fault scenarios. (a,b) are the results of Fault 1 and Fault 2.

With the influence of the current deviation, the SOC-based method's estimates have a downward trend, while the ICA-based method's estimates have an upward trend, compared with the results shown in Figure 5c. It should be noted that if the current deviation becomes large, the estimates from the ICA-based method will continue to move upward and the estimation error will become larger.

Compared with the single method, the estimation accuracy of the fusion method is not much improved. The main reason is that the ICA method outputs too few capacity estimates, which cannot provide continuous correction to estimates coming from the SOC-based method. Compared with the SOC-based method, the MaxAPEs of the fusion method under Fault 1 and Fault 2 are reduced by 0.392% and 0.474%, respectively, while the RMSEs under two fault conditions are reduced by 0.181% and 0.356%.

It is noticed that the difference between the three methods' estimation averages under the above scenarios is different. The difference between the three methods' estimation averages is slight for the normal conditions and conditions with a small current deviation. In contrast, for conditions with a large current deviation, the estimation average of the SOC-based and fusion method is close, while there is a significant deviation from that of the ICA-based method. To quantitatively describe the deviation between capacity estimates caused by inaccurate current information, the following criterion is proposed:

$$D_C = \max\left(\left|\frac{\bar{C}_m^{\text{SOC}} - \bar{C}_m^F}{\bar{C}_m^F}\right|, \left|\frac{\bar{C}_m^{\text{ICA}} - \bar{C}_m^F}{\bar{C}_m^F}\right|\right) \times 100\% \quad (13)$$

where D_C represents the capacity estimation deviation; \bar{C}_m^F , \bar{C}_m^{SOC} and \bar{C}_m^{ICA} mean the average during capacity fusion, SOC-based estimation, and ICA-based estimation.

Figure 8 shows the D_C for different cells under different current deviations. Note that with an increase in current deviation, the capacity estimation deviations both show a rising trend. Moreover, the more severe the battery aging, the higher the rising rate. It can be found that a threshold can be set to diagnose the fault condition of current inaccuracy. Here, we set this threshold to $T_C = 2\%$. Although the normal conditions and the slight fault conditions (10 mA deviation) of Cell 1 and Cell 2 cannot be distinguished from each other, the D_C of Cell 3 at the slight fault condition is larger than the set threshold. In addition, all the cells' D_C values are large than the set threshold. It is noted that the difference between the estimation averages will become larger with an increase in current deviation. Hence, it can be confirmed that a fault of current deviation can be identified when $D_C > T_C$ happens during capacity estimation and fusion.

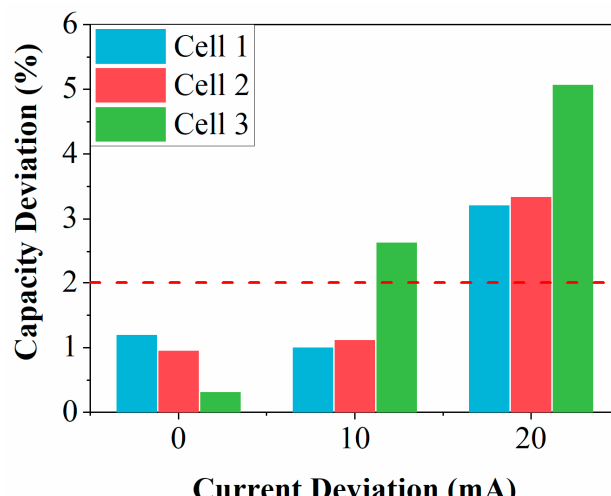


Figure 8. The capacity deviation for different cells.

5. Conclusion and Future Research Trends

Accurate and stable capacity acquisition has vital importance to the battery management technology in EVs. This study proposes an adaptive estimation–fusion method for battery capacity, utilizing more battery information and operating under complete battery operating conditions. The main conclusions of this study are drawn as follows:

(1) A general capacity fusion framework is proposed and then the SOC-based method and ICA-based method are revisited and employed during different operating conditions; further, the error covariance of different estimations is analyzed and derived.

(2) The adaptive battery fusion method is realized through the Kalman filter, which intelligently combines two estimates and takes advantage of estimation uncertainties.

(3) The fusion method outputs more accurate and stable capacity estimates. Owing to the utilization of more battery information, the maximum MaxAPE and RMSE are 2.547% and 1.703%, separately, under different aging statuses, which are smaller than traditional methods. Moreover, a judgment criterion based on capacity estimation and fusion for a sizeable current deviation fault is proposed.

Based on this research, there are several trends to be explored in future studies:

(1) More capacity estimates involved in fusion and more adaptive noise-matching methods in determining the process noise covariance will be helpful.

(2) Currently, the estimation during charging is the ICA-based method, which only updates four capacity estimates. A capacity estimation method with timely updating will continuously correct estimates from another method.

(3) The adaptability to different temperatures will be verified in further studies. Moreover, the estimation complexity caused by cell inconsistency shall be considered.

This study presents a detailed investigation of the application of information fusion technology in battery capacity estimation. For complex electrochemical systems, such as batteries, the information fusion technology will have more application scenarios, for example, battery multi-state estimation and remaining-life prediction. With the development of physical-based modeling and intelligent data-driven methods, as well as the availability of advanced-sensing techniques, information fusion will have diverse implementations and combinations to enhance the high-fidelity information acquisition from LIBs.

Author Contributions: Conceptualization, B.J. and H.D.; methodology, B.J.; software, B.J.; validation, B.J. and X.W.; formal analysis, B.J. and X.W.; investigation, B.J. and H.D.; data curation, B.J.; writing—original draft preparation, B.J. and X.W.; writing—review and editing, H.D.; visualization, B.J. and X.W.; supervision, H.D.; project administration, H.D.; funding acquisition, H.D. All authors have read and agreed to the published version of the manuscript.

Funding: This research was supported by the National Natural Science Foundation of China (NSFC, Grant No. U20A20310), Shanghai Sailing Program (Grant No. 22YF1450400), and China Postdoctoral Science Foundation (Grant No. 2022M712406).

Institutional Review Board Statement: Not applicable.

Informed Consent Statement: Not applicable.

Data Availability Statement: Not applicable.

Conflicts of Interest: The authors declare no conflict of interest.

References

1. Dai, H.; Jiang, B.; Hu, X.; Lin, X.; Wei, X.; Pecht, M. Advanced battery management strategies for a sustainable energy future: Multilayer design concepts and research trends. *Renew. Sustain. Energy Rev.* **2021**, *138*, 110480. [[CrossRef](#)]
2. Wang, X.; Wei, X.; Zhu, J.; Dai, H.; Zheng, Y.; Xu, X.; Chen, Q. A review of modeling, acquisition, and application of lithium-ion battery impedance for onboard battery management. *eTransportation* **2021**, *7*, 100093. [[CrossRef](#)]
3. Fasahat, M.; Manthouri, M. State of charge estimation of lithium-ion batteries using hybrid autoencoder and Long Short Term Memory neural networks. *J. Power Sources* **2020**, *469*, 228375. [[CrossRef](#)]
4. Moustafa, M.G.; Sanad, M.M.S. Green fabrication of ZnAl₂O₄-coated LiFePO₄ nanoparticles for enhanced electrochemical performance in Li-ion batteries. *J. Alloys Compd.* **2022**, *903*, 163910. [[CrossRef](#)]

5. Sanad, M.M.S.; Toghan, A. Unveiling the role of trivalent cation incorporation in Li-rich Mn-based layered cathode materials for low-cost lithium-ion batteries. *Appl. Phys. A* **2021**, *127*, 1–15. [[CrossRef](#)]
6. Hu, X.; Che, Y.; Lin, X.; Deng, Z. Health Prognosis for Electric Vehicle Battery Packs: A Data-Driven Approach. *IEEE/ASME Trans. Mechatron.* **2020**, *25*, 2622–2632. [[CrossRef](#)]
7. Wang, X.; Wei, X.; Dai, H. Estimation of state of health of lithium-ion batteries based on charge transfer resistance considering different temperature and state of charge. *J. Energy Storage* **2019**, *21*, 618–631. [[CrossRef](#)]
8. Li, X.; Wang, Z.; Zhang, L. Co-estimation of capacity and state-of-charge for lithium-ion batteries in electric vehicles. *Energy* **2019**, *174*, 33–44. [[CrossRef](#)]
9. Jiang, B.; Dai, H.; Wei, X.; Jiang, Z. Multi-kernel Relevance Vector Machine with Parameter Optimization for Cycling Aging Prediction of Lithium-ion Batteries. *IEEE J. Emerg. Sel. Top. Power Electron.* **2021**, *1*–12. [[CrossRef](#)]
10. Goh, T.; Park, M.; Seo, M.; Kim, J.G.; Kim, S.W. Successive-approximation algorithm for estimating capacity of Li-ion batteries. *Energy* **2018**, *159*, 61–73. [[CrossRef](#)]
11. Farmann, A.; Waag, W.; Marongiu, A.; Sauer, D.U. Critical review of on-board capacity estimation techniques for lithium-ion batteries in electric and hybrid electric vehicles. *J. Power Sources* **2015**, *281*, 114–130. [[CrossRef](#)]
12. Berecibar, M.; Gandiaga, I.; Villarreal, I.; Omar, N.; Van Mierlo, J.; Van den Bossche, P. Critical review of state of health estimation methods of Li-ion batteries for real applications. *Renew. Sustain. Energy Rev.* **2016**, *56*, 572–587. [[CrossRef](#)]
13. Xiong, R.; Li, L.; Tian, J. Towards a smarter battery management system: A critical review on battery state of health monitoring methods. *J. Power Sources* **2018**, *405*, 18–29. [[CrossRef](#)]
14. Schwunk, S.; Armbruster, N.; Straub, S.; Kehl, J.; Vetter, M. Particle filter for state of charge and state of health estimation for lithium-iron phosphate batteries. *J. Power Sources* **2013**, *239*, 705–710. [[CrossRef](#)]
15. Einhorn, M.; Conte, F.V.; Kral, C.; Fleig, J. A method for online capacity estimation of lithium ion battery cells using the state of charge and the transferred charge. *IEEE Trans. Ind. Appl.* **2012**, *48*, 736–741. [[CrossRef](#)]
16. Zhou, Z.; Cui, Y.; Kong, X.; Li, J.; Zheng, Y. A fast capacity estimation method based on open circuit voltage estimation for $\text{LiNi}_{x}\text{Co}_{y}\text{Mn}_{1-x-y}$ battery assessing in electric vehicles. *J. Energy Storage* **2020**, *32*, 101830. [[CrossRef](#)]
17. Zou, Y.; Hu, X.; Ma, H.; Li, S.E. Combined state of charge and state of health estimation over lithium-ion battery cell cycle lifespan for electric vehicles. *J. Power Sources* **2015**, *273*, 793–803. [[CrossRef](#)]
18. Wei, Z.; Leng, F.; He, Z.; Zhang, W.; Li, K. Online state of charge and state of health estimation for a lithium-ion battery based on a data-model fusion method. *Energies* **2018**, *11*, 1810. [[CrossRef](#)]
19. Xiong, R.; Sun, F.; Chen, Z.; He, H. A data-driven multi-scale extended Kalman filtering based parameter and state estimation approach of lithium-ion polymer battery in electric vehicles. *Appl. Energy* **2014**, *113*, 463–476. [[CrossRef](#)]
20. Kim, I.L.S. A technique for estimating the state of health of lithium batteries through a dual-sliding-mode observer. *IEEE Trans. Power Electron.* **2010**, *25*, 1013–1022. [[CrossRef](#)]
21. Hua, Y.; Cordoba-Arenas, A.; Warner, N.; Rizzoni, G. A multi time-scale state-of-charge and state-of-health estimation framework using nonlinear predictive filter for lithium-ion battery pack with passive balance control. *J. Power Sources* **2015**, *280*, 293–312. [[CrossRef](#)]
22. Wei, Z.; Zhao, J.; Ji, D.; Tseng, K.J. A multi-timescale estimator for battery state of charge and capacity dual estimation based on an online identified model. *Appl. Energy* **2017**, *204*, 1264–1274. [[CrossRef](#)]
23. Jiang, B.; Dai, H.; Wei, X. A Cell-to-Pack State Estimation Extension Method Based on a Multilayer Difference Model for Series-Connected Battery Packs. *IEEE Trans. Transp. Electrif.* **2022**, *8*, 2037–2049. [[CrossRef](#)]
24. Li, Y.; Abdel-Monem, M.; Gopalakrishnan, R.; Berecibar, M.; Nanini-Maury, E.; Omar, N.; van den Bossche, P.; Van Mierlo, J. A quick on-line state of health estimation method for Li-ion battery with incremental capacity curves processed by Gaussian filter. *J. Power Sources* **2018**, *373*, 40–53. [[CrossRef](#)]
25. He, J.; Bian, X.; Liu, L.; Wei, Z.; Yan, F. Comparative study of curve determination methods for incremental capacity analysis and state of health estimation of lithium-ion battery. *J. Energy Storage* **2020**, *29*, 101400. [[CrossRef](#)]
26. Bian, X.; Liu, L.; Yan, J. A model for state-of-health estimation of lithium ion batteries based on charging profiles. *Energy* **2019**, *177*, 57–65. [[CrossRef](#)]
27. Zhang, S.; Zhai, B.; Guo, X.; Wang, K.; Peng, N.; Zhang, X. Synchronous estimation of state of health and remaining useful lifetime for lithium-ion battery using the incremental capacity and artificial neural networks. *J. Energy Storage* **2019**, *26*, 100951. [[CrossRef](#)]
28. Shen, S.; Sadoughi, M.; Chen, X.; Hong, M.; Hu, C. A deep learning method for online capacity estimation of lithium-ion batteries. *J. Energy Storage* **2019**, *25*, 100817. [[CrossRef](#)]
29. Deng, Z.; Hu, X.; Lin, X.; Xu, L.; Che, Y.; Hu, L. General Discharge Voltage Information Enabled Health Evaluation for Lithium-Ion Batteries. *IEEE/ASME Trans. Mechatron.* **2020**, *26*, 1295–1306. [[CrossRef](#)]
30. Hu, C.; Jain, G.; Zhang, P.; Schmidt, C.; Gomadam, P.; Gorka, T. Data-driven method based on particle swarm optimization and k-nearest neighbor regression for estimating capacity of lithium-ion battery. *Appl. Energy* **2014**, *129*, 49–55. [[CrossRef](#)]
31. Deng, Z.; Yang, L.; Cai, Y.; Deng, H.; Sun, L. Online available capacity prediction and state of charge estimation based on advanced data-driven algorithms for lithium iron phosphate battery. *Energy* **2016**, *112*, 469–480. [[CrossRef](#)]
32. Jiang, B.; Zhu, J.; Wang, X.; Wei, X.; Shang, W.; Dai, H. A comparative study of different features extracted from electrochemical impedance spectroscopy in state of health estimation for lithium-ion batteries. *Appl. Energy* **2022**, *322*, 119502. [[CrossRef](#)]

33. Tan, Y.; Zhao, G. Transfer learning with long short-term memory network for state-of-health prediction of lithium-ion batteries. *IEEE Trans. Ind. Electron.* **2020**, *67*, 8723–8731. [[CrossRef](#)]
34. Zheng, Y.; Qin, C.; Lai, X.; Han, X.; Xie, Y. A novel capacity estimation method for lithium-ion batteries using fusion estimation of charging curve sections and discrete Arrhenius aging model. *Appl. Energy* **2019**, *251*, 113327. [[CrossRef](#)]
35. Xiong, R.; Wang, J.; Shen, W.; Tian, J.; Mu, H. Co-Estimation of State of Charge and Capacity for Lithium-ion Batteries with Multi-Stage Model Fusion Method. *Engineering* **2021**, *7*, 1469–1482. [[CrossRef](#)]
36. Balasingam, B.; Avvari, G.V.; Pattipati, B.; Pattipati, K.R.; Bar-Shalom, Y. A robust approach to battery fuel gauging, part II: Real time capacity estimation. *J. Power Sources* **2014**, *269*, 949–961. [[CrossRef](#)]
37. Zhang, Y.; Jiang, C.; Yue, B.; Wan, J.; Guizani, M. Information fusion for edge intelligence: A survey. *Inf. Fusion* **2022**, *81*, 171–186. [[CrossRef](#)]
38. Qiao, D.; Wei, X.; Fan, W.; Jiang, B.; Lai, X.; Zheng, Y.; Tang, X.; Dai, H. Toward safe carbon-neutral transportation: Battery internal short circuit diagnosis based on cloud data for electric vehicles. *Appl. Energy* **2022**, *317*, 119168. [[CrossRef](#)]
39. Qiao, D.; Wang, X.; Lai, X.; Zheng, Y.; Wei, X.; Dai, H. Online quantitative diagnosis of internal short circuit for lithium-ion batteries using incremental capacity method. *Energy* **2021**, *243*, 123082. [[CrossRef](#)]
40. Jiang, B.; Dai, H.; Jiang, W.; Pei, F. A novel framework of multi-dimension capacity estimation and fusion for lithium-ion battery. In Proceedings of the 2020 IEEE Vehicle Power and Propulsion Conference (VPPC), Gijón, Spain, 26–29 October 2020.
41. Han, C.; Zhu, H.; Duan, Z. Estimation fusion. In *Multi-Source Information Fusion*, 2nd ed.; Tsinghua University Press: Beijing, China, 2010; pp. 250–319.
42. Jiang, B.; Dai, H.; Wei, X. Incremental capacity analysis based adaptive capacity estimation for lithium-ion battery considering charging condition. *Appl. Energy* **2020**, *269*, 115074. [[CrossRef](#)]
43. Jiang, B.; Dai, H.; Wei, X.; Xu, T. Joint estimation of lithium-ion battery state of charge and capacity within an adaptive variable multi-timescale framework considering current measurement offset. *Appl. Energy* **2019**, *253*, 13619. [[CrossRef](#)]
44. Wei, Z.; Zou, C.; Leng, F.; Soong, B.H.; Tseng, K.-J. Online model identification and state-of-charge estimate for lithium-ion battery with a recursive total least squares-based observer. *IEEE Trans. Ind. Electron.* **2018**, *65*, 1336–1346. [[CrossRef](#)]
45. Kim, T.; Wang, Y.; Sahinoglu, Z.; Wada, T.; Hara, S.; Qiao, W. A Rayleigh Quotient-based recursive total-least-squares online maximum capacity estimation for lithium-ion batteries. *IEEE Trans. Energy Convers.* **2015**, *30*, 842–851. [[CrossRef](#)]
46. Pastor-Fernández, C.; Uddin, K.; Chouchelamane, G.H.; Widanage, W.D.; Marco, J. A comparison between electrochemical impedance spectroscopy and incremental capacity-differential voltage as li-ion diagnostic techniques to identify and quantify the effects of degradation modes within battery management systems. *J. Power Sources* **2017**, *360*, 301–318. [[CrossRef](#)]
47. Dubarry, M.; Beck, D. Analysis of Synthetic Voltage vs. Capacity Datasets for Big Data Li-ion Diagnosis and Prognosis. *Energies* **2021**, *14*, 2371. [[CrossRef](#)]
48. Dubarry, M.; Berecibar, M.; Devie, A.; Anseán, D.; Omar, N.; Villarreal, I. State of health battery estimator enabling degradation diagnosis: Model and algorithm description. *J. Power Sources* **2017**, *360*, 59–69. [[CrossRef](#)]
49. Crassidis, J.L.; Cheng, Y. Error-covariance analysis of the total least-squares problem. *J. Guid. Control. Dyn.* **2014**, *37*, 1053–1063. [[CrossRef](#)]
50. Ramachandran, K.M.; Tsokos, C.P. Linear regression models. In *Mathematical Statistics with Applications in R*, 3rd ed.; Academic Press: Cambridge, MA, USA, 2021; pp. 301–341.
51. Fang, Q.; Wei, X.; Dai, H. A Remaining Discharge Energy Prediction Method for Lithium-Ion Battery Pack Considering SOC and Parameter Inconsistency. *Energies* **2019**, *12*, 987. [[CrossRef](#)]
52. You, H.; Zhu, J.; Wang, X.; Jiang, B.; Sun, H.; Liu, X.; Wei, X.; Han, G.; Ding, S.; Yu, H.; et al. Nonlinear health evaluation for lithium-ion battery within full-lifespan. *J. Energy Chem.* **2022**, *72*, 333–341. [[CrossRef](#)]